

Article

Destabilization of NaBH₄ by Transition Metal Fluorides

Isabel Llamas Jansa * , Georgios N. Kalantzopoulos † , Kari Nordholm and Bjørn C. Hauback

Department for Neutron Characterization, Institute for Energy Technology, P.O. Box 40, NO-2027 Kjeller, Norway; georgios.kalantzopoulos@kjemi.uio.no (G.N.K.); kari.kj.no88@gmail.com (K.N.); Bjorn.Hauback@ife.no (B.C.H.)

* Correspondence: isabel.llamas@ife.no

† Current address: Department of Chemistry, University of Oslo, P.O. Box 1033, NO-0315 Oslo, Norway.

Received: 24 September 2019; Accepted: 5 February 2020; Published: 12 February 2020



Abstract: With the goal of improving performance of a hydrogen-rich storage medium, the influence of a collection of first and second period transition metal fluorides on the destabilization of NaBH₄ is studied on samples produced by ball milling NaBH₄ with 2 mol% of a metal fluoride additive. The effects obtained by increasing additive amount and changing oxidation state are also evaluated for NbF₅, CeF₃, and CeF₄. The as-milled products are characterized by in-house power X-ray diffraction, while the hydrogen release and decomposition are monitored by temperature programmed desorption with residual gas analysis, differential scanning calorimetry, and thermogravimetry. The screening of samples containing 2 mol% of additive shows that distinctive groups of transition metal fluorides affect the ball milling process differently depending on their enthalpy of formation, melting point, or their ability to react at the temperatures achieved during ball milling. This leads to the formation of NaBF₄ in the case of TiF₄, MnF₃, VF₄, CdF₂, NbF₅, AgF, and CeF₃ and the presence of the metal in CrF₃, CuF₂, and AgF. There is no linear correlation between the position of the transition metal in the periodic table and the observed behavior. The thermal behavior of the products after milling is given by the remaining NaBH₄, fluoride, and the formation of intermediate metastable compounds. A noticeable decrease of the decomposition temperature is seen for the majority of the products, with the exceptions of the samples containing YF₃, AgF, and CeF₃. The largest decrease of the decomposition temperature is observed for NbF₅. When comparing increasing amounts of the same additive, the largest decrease of the decomposition temperature is observed for 10 mol% of NbF₅. Higher amounts of additive result in the loss of the NaBH₄ thermal signal and ultimately the loss of the crystalline borohydride. When comparing additives with the same transition metal and different oxidation states, the most efficient additive is found to be the one with a higher oxidation state. Furthermore, among all the samples studied, higher oxidation state metal fluorides are found to be the most destabilizing agents for NaBH₄. Overall, the present study shows that there is no single parameter affecting the destabilization of NaBH₄ by transition metal fluorides. Instead, parameters such as the transition metal electronegativity and oxidation state or the enthalpy of formation of the fluoride and its melting point are competing to influence the destabilization. In particular, it is found that the combination of a high metal oxidation state and a low fluoride melting point will enhance destabilization. This is observed for MnF₃, NbF₅, NiF₂, and CuF₂, which lead to high gas releases from the decomposition of NaBH₄ at the lowest decomposition temperatures.

Keywords: sodium borohydride; transition metal fluoride; hydrogen storage; destabilization; additives; future fuels; renewable energy

1. Introduction

As hydrogen becomes one of the important alternative energy carriers for renewable energy sources, the discussion about its safe and efficient storage gains momentum. The challenge is not only to achieve small compact systems with high gravimetric and volumetric hydrogen densities fulfilling the necessary safety requirements, but for a competitive practical use, the hydrogen needs to be efficiently absorbed and desorbed. These goals can be reached by utilizing storage media that have intrinsically high hydrogen densities such as pressurized cylinders and cryogenic liquid hydrogen systems, as well as by solid-state hydrogen containing materials. The latter method has the additional advantages of safety and high volumetric density [1–7].

Among solid-storage materials, first and second group borohydrides (LiBH_4 , NaBH_4 , $\text{Ca}(\text{BH}_4)_2$, and $\text{Mg}(\text{BH}_4)_2$) [8–12] have been for two decades very attractive candidates because of their gravimetric densities of the order of 10 to 20 wt% H_2 [13–15]. NaBH_4 , which has a high gravimetric capacity of 10.6 wt% and a decomposition temperature of about 535 °C [16], has gone from being a favorite solid-storage material in the early 2000s to being rejected by the U.S. Department of Energy (DoE) [17] for on-board applications, to then again being described as a fuel for the future [18] due to its large yields of hydrogen release by hydrolysis and thermal decomposition that can be readily used in aqueous solutions in some types of fuel cells such as proton exchange membrane fuel cells (PEMFCs) or direct boron hydride fuel cells (DBFCs) [18–21].

The present work focuses on reducing the thermal desorption temperature of NaBH_4 below 535 °C by adding small amounts of transition metal fluorides (TMFs). This is an extension of two previous works: one with transition metal chlorides (TMCs) that showed the formation of NaBH_4 -chloride substituted phases [22] and another with selected TMFs, where no substitution was found [23].

An extensive literature review including the last four decades reveals a limited amount of work concerning the effect of fluorides on borohydrides. The first report of a borohydride being ball-milled with a variety of fluorides corresponds to Zhang et al. [24]. In this work, selected chlorides were found to form new borohydrides easier than their corresponding fluorides. Al-Kukhun et al. [25] and Zhang et al. [26] also found that the addition of selected fluorides (NbF_5 and CaF_2 and ZnF_2 and TiF_3 , respectively) to MgBH_4 had a positive effect on the hydrogen release and the kinetics of the borohydride. Furthermore, Minella et al. [27] investigated the sorption properties and reversibility of the Ti(IV) and Nb(V) doped- $(\text{CaBH}_4)_2\text{-MgH}_2$ system. Adding NbF_5 resulted in a system with enhanced reversibility by slightly suppressing the formation of $\text{CaB}_{12}\text{H}_{12}$. Likewise, Zhou et al. [28] used CeF_3 as a catalyst on LiBH_4 nanoconfined on activated carbon. They found a considerable decrease of the onset temperature of hydrogen release and a substantial increase in the dehydrogenation capacity. The fluoride substitution of LiBH_4 by Richter et al. [29] was one of the most significant destabilization effects of fluorides on borohydrides observed up to date.

The first study involving NaBH_4 and fluorides did not occur until early 2013 when Rude et al. [30] reported fluorine substitution on NaBH_4 while investigating different $\text{NaBH}_4\text{-NaBF}_4$ mixtures. The fluorine-substituted phases were found to decompose into more stable compounds, while the $\text{NaBH}_4\text{-NaBF}_4$ composite itself presented considerably lower decomposition temperature. Chong et al. [31] found that the addition of LaF_3 to NaBH_4 promoted hydrogen sorption better than LaH .

The literature about the co-addition of more than one transition metal fluoride to a borohydride is rare. Recently, Huang et al. [32] found that adding ScF_3 and YF_3 to a NaBH_4 -containing system resulted in a three step hydrogen desorbing system with enhanced reversibility when using the two fluorides simultaneously. The results were partially confirmed by Zhao et al. [33] on the reversibility of $3\text{NaBH}_4/\text{ScF}_3$ and by Huang et al. [34] on the reversible hydrogen sorption behavior of $3\text{NaBH}_4\text{-}(x)\text{YF}_3\text{-}(1-x)\text{GdF}_3$. A recent review by Jain et al. [35] summarized the catalytic effect on lightweight hydrogen storage materials of a variety of compounds, including TiF_3 , TiF_4 , CeF_4 , NbF_5 , ZrF_4 , ternary K-TM-F fluorides (TM: Ti, Zr, Ni, Fe), NaMgF_3 , and NaF .

Additionally, Mao et al. [36] concluded that using metal fluorides as additives is a promising direction for improving the sorption kinetics of NaBH₄ by lowering the energy barriers. These authors stated that both Ti and F have a positive effect. However, the physical, chemical, or thermodynamic parameters of the halide responsible for the increase in the decomposition rate of NaBH₄/borohydrides/hydrides have so far not been identified. It is generally suggested that the oxidation state of the metal element that forms the halide plays the most important role. This is justified by the influence of different catalysts observed for chemical compounds that exist in only one oxidation state when comparing to chemical compounds with multivalent metals [37,38]. Similar discussions have been carried out about the influence of the oxidation state of the metal for catalyzed MgH₂ [39,40].

All these studies showed that some metal fluorides induce strong effects on the destabilization of particular borohydrides. However, there is still a large number of fluorides whose effect on borohydrides has not been reported that might be beneficial for the hydrogen storage community. Continuing with this line of investigation, the main focus of the present work is to study the destabilization effects of available transition metal fluorides (TMFs) from the first and second periods of the periodic table on NaBH₄. These effects might occur through the formation of new compounds, as well as the mechanochemical process itself.

The ball-milled products are analyzed by powder X-ray diffraction (PXD) and a variety of thermal methods including differential scanning calorimetry (DSC) and temperature-programmed desorption (TPD). The observed behavior is discussed in terms of the transition metal (TM) electronic structure and the position in the periodic table, as well as the ability of the fluoride to react during milling and form new compounds.

Variations due to the additive amount and oxidation state are also discussed. In particular, NbF₅ was chosen as one of the additives based on previous results by Luo et al. [41] showing an increase of solubility during ball milling due to its low melting point (90 °C). On the other hand, increasing the oxidation state of a metal has been shown to lead to compounds with a lower melting point and, therefore, higher solubility during the ball milling process [41]. This is tested by using CeF₃ and CeF₄ as additives to NaBH₄.

2. Results and Discussion

2.1. Ball Milling Effects of the TMFs on NaBH₄

Table 1 summarizes the PXD data obtained for all the samples after ball milling and analyzed by DIFFRAC plus EVA in terms of the wt% content of the different compounds in the mixture. The table also contains the calculated wt% of the original mixtures for comparison. The same data are included in Appendix A as PXD plots (Figure A1). The data showed that all the samples still contained crystalline NaBH₄ in large amounts after milling, although the exact composition of the products varied depending on the TM fluoride. Moreover, the lack of a shift in the Bragg peaks corresponding to the remaining NaBH₄ indicated that there was no substitution in the NaBH₄ unit cell despite the presence of crystalline NaBF₄ in some of the samples. This was in agreement with the previously reported formation of NaBF₄ [23].

The added fluorides remained as a crystalline phase for ScF₃, FeF₃, CrF₃, NiF₃, CoF₃, CuF₂, VF₄, ZnF₂, CdF₂, YF₃, and AgF. With the exception of AgF and VF₄, these were all fluorides with melting points above 800 °C. On the other hand, TiF₄, MnF₃, NbF₅, ZrF₄, CeF₄, and CeF₃ did not appear as crystalline phases in the PXD results, and no peaks corresponding to NbF₅ were seen in the 10 and 15 mol% cases either. Except for the ZrF₄ and CeF₄ containing samples, which only showed crystalline NaBH₄ in the PXD pattern, the disappearance of the fluoride in these samples was correlated with the appearance of NaBF₄ and/or metallic TM. The presence of other compounds containing TM and fluorine could not be confirmed with the current PXD data.

Table 1. Composition of the samples before and after ball milling. The first 5 columns show the composition of the ball-milled samples as evaluated by EVA. The two last columns are the calculated wt% of the original physical mixture before ball milling.

Sample	NaBH ₄ (wt%)	TMF (wt%)	NaBF ₄ (wt%)	TM (wt%)	Other (wt%)	NaBH ₄ (wt%)	TMF (wt%)
ScF ₃	95.5	4.5				94.9	5.1
TiF ₄	82.0		18.0			93.9	6.2
VF ₄	77.9	3.6	18.5			93.7	6.3
CrF ₃	95.7	4.0		0.4		94.6	5.5
MnF ₃	55.3		44.7			94.4	5.6
FeF ₃	94.9	5.1				94.4	5.6
CoF ₃	95.8	3.2			1.0	94.2	5.8
NiF ₂	94.5	5.5				95.1	4.9
CuF ₂	88.8	9.8		1.4		94.9	5.1
ZnF ₂	95.1	4.9				94.8	5.2
YF ₃	92.5	7.5				92.8	7.2
ZrF ₄	100					91.9	8.1
NbF ₅ (2 mol%)	88.1		4.6		2.8	91.0	9.0
NbF ₅ (10 mol%)	70.2		8.0		2.4	66.8	33.2
NbF ₅ (15 mol%)	59.0		10.6		2.6	57.3	42.7
AgF	93.7	0.8	2.9	1.0	1.5	93.7	6.3
CdF ₂	90.5	6.6	2.9			92.6	7.4
CeF ₃	97.6		2.4			90.6	9.4
CeF ₄	100					89.8	10.3

A detailed analysis of the PXD patterns suggested a classification of the samples based on the products of the ball milling. First, ScF_3 , FeF_3 , NiF_2 , ZnF_2 , and YF_3 showed no effect on the milling process. For these additives, the original ratio between NaBH_4 and the fluoride was still present in the powder after ball milling. Small changes of the composition appeared for the samples containing CrF_3 , CoF_3 , and CuF_2 . This was seen by the presence of metallic Cr and Cu, respectively, while for CoF_3 , the presence of CoF_2 was likely related to the original fluoride. Stronger changes of the composition were introduced by CdF_2 , CeF_3 , and AgF . In these cases, NaBF_4 was present in the products together with the original NaBH_4 and the fluoride. For the AgF case, metallic Ag and Ag_2F were also seen in the PXD pattern.

TiF_4 , MnF_3 , VF_4 , and NbF_5 (2, 10, and 15 mol%) produced the strongest changes of the composition of the samples after milling. This was mostly seen for TiF_4 , MnF_3 , and VF_4 by a significant amount of NaBF_4 and for VF_4 by the additional metallic V. For the NbF_5 cases, the amount of NaBF_4 produced by milling was smaller than published earlier [23]. On the other hand, two new compounds containing Nb appeared in these samples: NbF_3 and $\text{NaNb}_{1.25}\text{F}_6$. The content of these two products increased with NbF_5 content in the mixture. The presence of F^- containing compounds in some of the studied cases confirmed the decomposition of the original fluorides and some level of H^- substitution in small amounts of NaBH_4 .

In contrast, CeF_4 and ZrF_4 containing samples showed only crystalline NaBH_4 after milling, with the exception of a nonsymmetric peak at 25° for CeF_4 indicating a substituted phase. The comparison of the composition of the samples with CeF_3 and CeF_4 after milling showed that both oxidation states led to the disappearance of the fluoride in the crystalline form. Moreover, for CeF_3 , the analysis showed that the fluoride decomposed to form NaBF_4 , while for CeF_4 , there was no crystalline indication of the fluoride dissociating (it could still be there as amorphous). The effect of the oxidation state could also be seen by comparing the reported use of TiF_3 [23] and the current use of TiF_4 . While the published data showed no formation of a new crystalline phase after ball milling for 3 h, the current data showed the formation of up to 18 wt% of NaBF_4 after only 1 h ball milling, when using the higher oxidation state.

Overall, the melting point of the fluoride seemed to play a role in the interaction with NaBH_4 during ball milling. This was easily seen in the case of NbF_5 , but also in the general trends observed between samples that contained high melting point TM fluorides such as ScF_3 and NiF_2 , which led to mostly unchanged sample compositions, and those with lower melting points such as TiF_4 and VF_4 , which led to the formation of NaBF_4 . However, the PXD results alone did not establish any correlation between the ability of the fluoride to interact chemically with NaBH_4 and properties such as the enthalpy of formation, the electronic structure, or the oxidation state of the TM.

2.2. Effect of TMFs on the Destabilization of NaBH_4

2.2.1. Pure NaBH_4 with Different Calorimetry Methods

Pure NaBH_4 samples were analyzed with three different calorimetric methods: TPD, DSC-Netzsch and DSC-Setaram, and TGA (Figure 1). Each of these techniques accessed useful information and presented experimental limitations that might lead to different decomposition behaviors of the samples.

The in-house TPD and the Netzsch DSC (blue and black lines in Figure 1) showed the maximum of the melting point of NaBH_4 to occur at around 503°C , in agreement with the literature.

However, the decomposition event happened at higher temperatures with the Netzsch DSC, at about 558°C , compared to the 534°C of the TPD curve. The reason for this discrepancy was the fact that the TPD analysis was taking place in a dynamic vacuum, while the Netzsch DSC measured under an Ar flow of 20 mL/min. The Ar flow cooled down the surroundings of the sample, making it more difficult to achieve the necessary temperature to decompose (more heat needed to be applied to decompose the material).

Larger differences were observed between these two techniques and the Setaram DSC analysis. On the one hand, the Setaram DSC technique only showed the NaBH_4 melting event at 509 °C. The reason for this was that the measurements were generally carried out in closed stainless steel (SS) crucibles. These were high pressure crucibles without a venting hole, and therefore, it was likely that the desorbed gas/ H_2 built pressure inside the crucible and hindered the gas evolution, stopping the decomposition process. On the other hand, the melting point was observed to happen at about 6 °C higher than by the TPD and Netzscht techniques. The reason for this shift was related to both the different experimental environments (vacuum and Ar flows of 15 and 20 mL/min) and the different equilibrium pressure imposed by the closed crucible.

The TGA data showed the expected single-step decomposition corresponding to H_2 to maximize beyond 600 °C and with its onset at 505 °C.

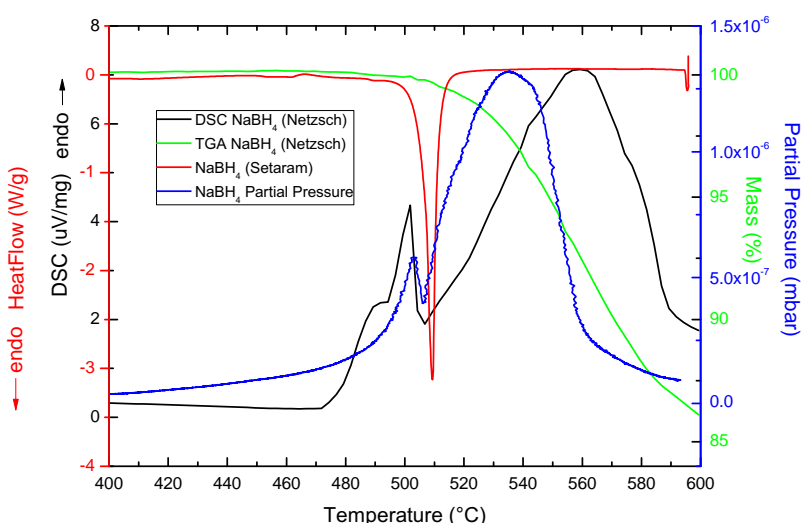


Figure 1. Comparison of the different calorimetry and gravimetric methods used to measure NaBH_4 . Black: DSC-Netzscht in $\mu\text{V}/\text{mg}$; red: DSC-Setaram in W/g ; blue: TPD in mbar of H_2 ; green: TGA in mass % of H_2 .

2.2.2. Temperature-Programmed Desorption Results

Table 2 summarizes the data obtained by TPD for all the samples. The most important peaks were the main decomposition and melting events of NaBH_4 . Furthermore, Figure 2 shows the influence of the TM fluoride additive on the NaBH_4 decomposition temperature as measured by TPD and represented as the difference in the temperature between the decomposition peak of the sample with additive and that of pure NaBH_4 .

As seen in the figure, prominent reductions in the decomposition temperature corresponded to MnF_3 , CuF_2 , NiF_2 , and NbF_5 , with the largest reduction for 10 and 15 mol% NbF_5 , where the decomposition already occurred at 379 °C. The least influence on the decomposition behavior of NaBH_4 was observed for TiF_4 and YF_3 .

However, this destabilization performance could not be correlated to a single fluoride property. On the one hand, MnF_3 , CuF_2 , and NiF_2 had a relatively high enthalpy of formation, ΔE_{form} , suggesting that less energy was required to mix and react with the borohydride. On the other hand, NbF_5 had the highest metal oxidation state and the lowest fluoride melting point. The latter property had a strong effect during ball milling as it enhanced the effective surface area for reactions between the fluoride and the borohydride to occur. The high oxidation state of the metal then provided an electronic environment with an abundance of available e^- to assist in further chemical reactions.

Table 2. TPD temperatures for the main decomposition and melting events of all the samples together with their temperature difference when comparing to NaBH₄. The tabulated values correspond to the maxima of the measured data in every peak region. The samples are ordered from top to bottom following Figure 2.

Sample	Decomposition °C	Difference °C	Melting °C	Difference °C
NaBH ₄	535	0	503	0
TiF ₄	522	13	452	51
YF ₃	513	22	462	41
CdF ₂	512	23	461	42
CeF ₃	506	29	487	16
ZnF ₂	504	31	460	43
ZrF ₄	503	32	460	43
CeF ₄	502	33	457	46
CoF ₃	501	34	452	51
ScF ₃	501	34	455	48
CrF ₃	500	35	464	39
VF ₄	499	36	452	51
FeF ₃	498	37	460	43
AgF	498	37	466	37
MnF ₃	483	52	453	50
CuF ₂	476	59	425	78
NiF ₂	452	83	446	57
NbF ₅ (2 mol%)	442	93	190	313
NbF ₅ (10 mol%)	379	156	315	188
NbF ₅ (15 mol%)	379	156	315	188

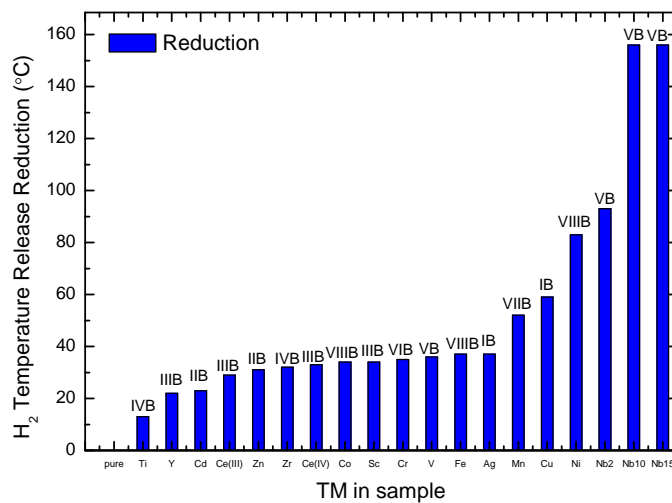


Figure 2. Temperature difference between the main decomposition peak of the samples with additives and that of pure NaBH₄ as observed by TPD.

By increasing the amount of NbF₅ additive from 2 to 10 mol%, the decomposition temperature of the remaining NaBH₄ decreased from 442 to 379 °C. Larger amounts of fluoride additive led to no change in the decomposition features, indicating that there was an optimal amount of additive of 10 to 15 mol% before NaBH₄ disappears.

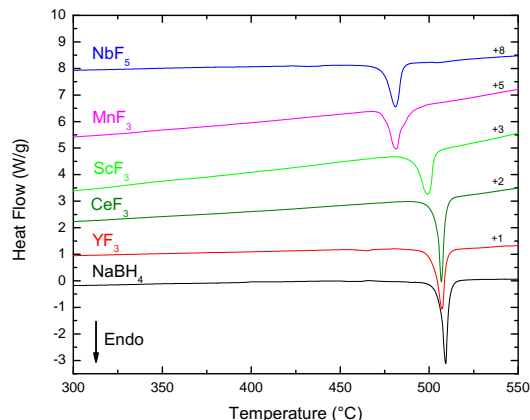
The influence of different oxidation states was represented by the CeF₃ and CeF₄ cases. For these samples, the TPD data showed that the TM with higher oxidation state resulted in a slightly higher decomposition temperature.

The TPD signals corresponding to diborane species ($m/z = 26, 27$) were found to be two orders of magnitude weaker than those for hydrogen ($m/z = 2$) for the whole temperature range and for all the investigated samples. No indication of fluoride release was found. Overall, the hydrogen release temperature could not be correlated with the Pauling electronegativity of the TM ($\chi\rho$) as it was reported for selected TM chlorides on a study on NH_3BH_3 [42].

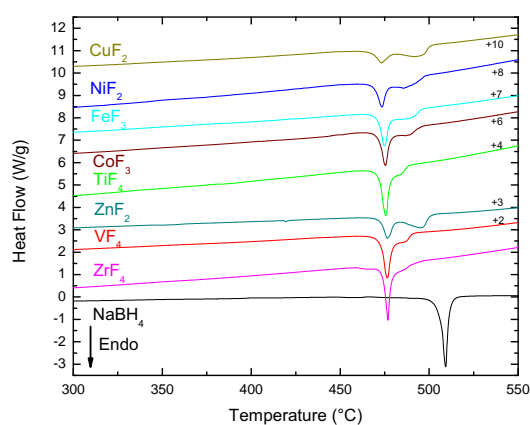
2.2.3. Closed Crucible DSC-Setaram Discussion

As discussed in Section 2.2.1, DSC-Setaram data of pure NaBH_4 showed a strong endothermic event occurring at 509°C that corresponded with melting. Since the Setaram measurements were done in closed SS crucibles (closed system), the decomposition event at higher temperatures was hindered and not seen. The same effect was expected for the samples containing fluoride additives. In Figure 3, the samples are grouped based on DSC-Setaram measurements.

ScF_3 , YF_3 , and CeF_3 showed a single endothermic peak attributed to the melting of NaBH_4 , but occurring at slightly lower temperatures (NaBH_4 $509^\circ\text{C} > \text{YF}_3$ $507^\circ\text{C} \geq \text{CeF}_3$ $507^\circ\text{C} > \text{ScF}_3$ 499°C).



(a) Group 1



(b) Group 2

Figure 3. Cont.

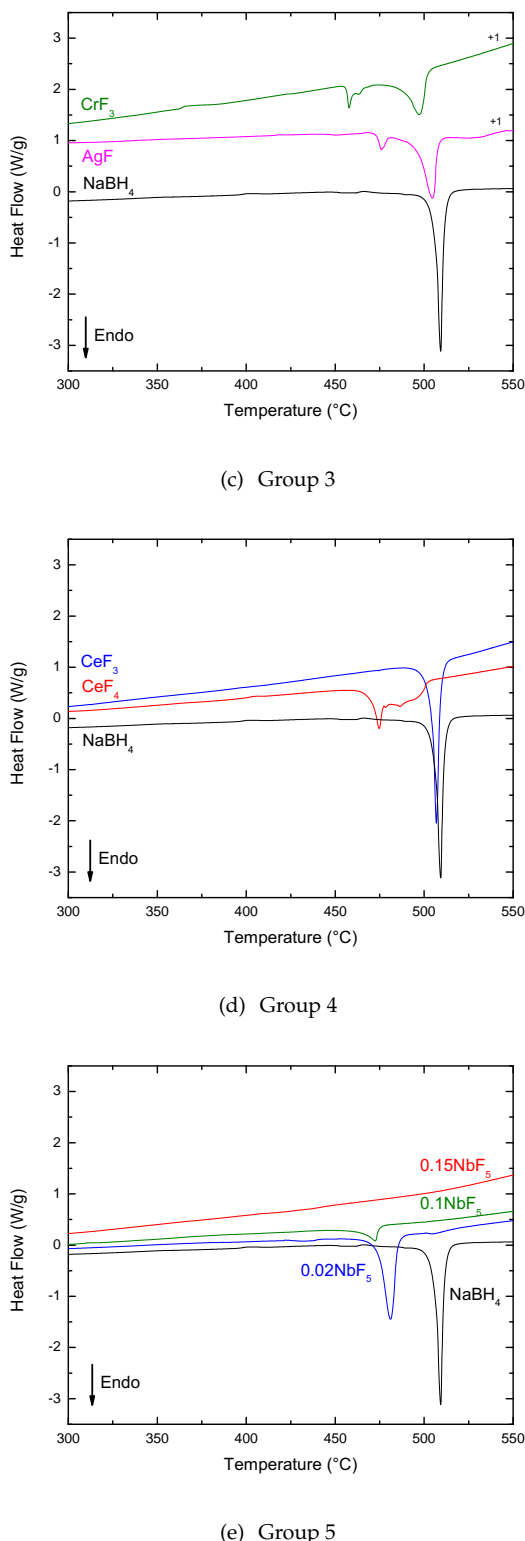


Figure 3. DSC-Setaram corresponding to the samples distributed in different groups based on their behavior. The numbers on the right-hand side indicate the shift applied to the data for plotting.

The ScF_3 melting feature was broader and asymmetric compared to the narrower peaks of YF_3 and CeF_3 . From the PXD data in Section 2.1, it was found that the first two samples contained metallic Sc and Y, respectively, but no indications of metallic Ce were observed. Thus, the presence of metallic

TM (Sc or Y, respectively) did not explain the different melting profiles. Moreover, the presence of metallic TM did not seem to influence the melting of NaBH₄ as seen by DSC-Setaram. On the other hand, the asymmetry of some melting peaks could be interpreted as the overlapping of the melting of NaBH₄ with other intermediate phases formed during heating, as well as by a small gas release, which was weakened in the SS closed system.

The same asymmetry was seen in the DSC-Setaram of MnF₃ and NbF₅, which still appeared as single peaks, but at much lower temperatures than the melting point of pure NaBH₄ (481.5 °C and 481 °C, respectively). These were samples that contained NaBF₄ (Table 1), which crystallized in a different space group than NaBH₄ and seemed to have a prominent effect on the melting point. In the case of MnF₃, shoulders at both sides of the main peak also indicated the overlapping of events related to the presence of different phases and hindered gas release.

The second group of samples (Group 2 in Figure 3) showed a strong decrease of the melting temperature of the ball-milled samples, which now appeared between 473 and 477 °C. In addition, the range of melting temperatures in this group showed a different level of interaction between the TM fluoride additives and NaBH₄ and their role in disturbing the intermolecular forces in the borohydride. The samples also showed similar second features after the melting peak, between 482 °C at the shoulder in TiF₄ and the single peak at 496 °C in ZnF₂. This second feature occurred at too low temperatures to be associated with NaBH₄ decomposition, which was also hindered by the SS crucibles, avoiding gas release. Therefore, it could only be interpreted as processes occurring on intermediate phases created in the mixture during heating. This was also confirmed by the fact that as the intensity of the melting feature decreased, the stronger the feature at larger temperatures became, indicating that some of the NaBH₄ in the mixture after milling reacted during heating.

A different behavior was seen in the DSC-Setaram of the remaining samples, AgF and CrF₃. Their melting points were not strongly changed from that of NaBH₄, suggesting a small effect by the presence of NaBF₄ after milling with AgF. On the other hand, features at lower temperatures than their melting peaks indicated the presence of other intermediate phases and processes happening during the low temperature stages of heating.

All in all, the majority of the fluorides studied in this work had an influence on the melting temperature of NaBH₄. This was particularly true for all the second period TMFs, but also for MnF₃ and NbF₅.

The least effective in decreasing the melting temperature, as measured by DSC-Setaram, were YF₃ and CeF₃, and the most effective were MnF₃, NbF₅, NiF₂, and CuF₂. These latter fluorides were the same fluorides that led to the highest hydrogen releases as observed by TPD (Figure 2).

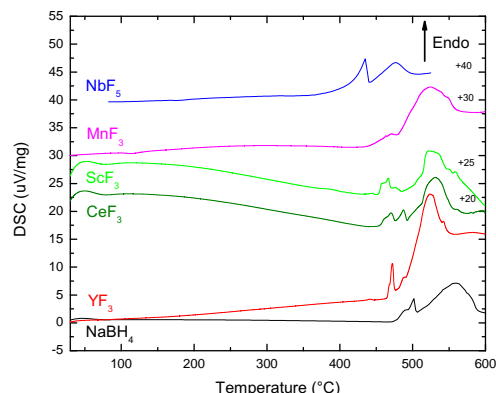
The DSC-Setaram data also showed a significant difference between the CeF₃ and CeF₄ samples (Group 4 in Figure 3). While the lower oxidation state compound only decreased the melting temperature of NaBH₄ slightly, the higher oxidation state showed a feature at 475 °C that could be assigned to the melting and a broad region of overlapping events between 477 and 500 °C. The comparison between the DSC-Setaram behavior of CeF₄ and the other tetravalent fluorides, VF₄ and ZrF₄ (Figure 3, Group 2) showed that CeF₄ had a smaller effect on the melting point of NaBH₄. In the case of the trivalent fluorides, MnF₃, FeF₃, and CoF₃ showed the strongest decrease of the melting point (close to 475 °C), while CrF₃ and ScF₃ showed a smaller effect and CeF₃ and YF₃ the smallest effect.

On the other hand, the increase of NbF₅ content in the mixture had the effect of reducing the intensity of the melting peak, as well as reducing the melting temperature. For the 15 mol% NbF₅ sample, the melting peak in the DSC-Setaram disappeared completely, indicating that the amount of NaBH₄ available was small (Group 5 in Figure 3). This was confirmed by the PXD data, which showed a decrease in the content of NaBH₄ after ball milling of about 40 % or ca. 59 wt% (Table 1).

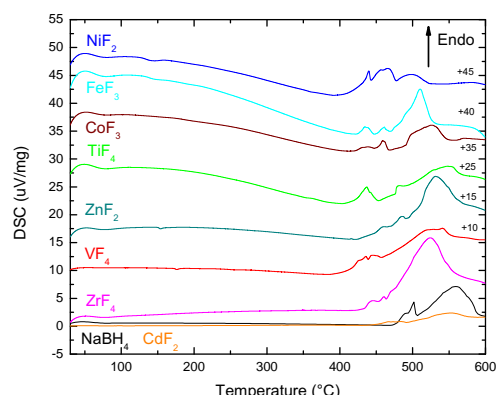
2.2.4. DSC-Netzsch Discussion

DSC-Netzsch data complemented the findings by TPD and DSC-Setaram by showing the different calorimetric events during heating in the milled samples as presented in Figure 4.

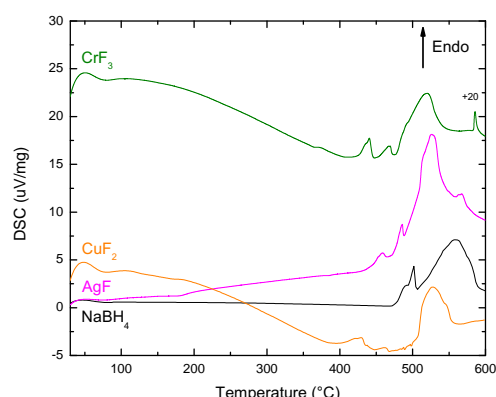
Both TPD and DSC-Netzsch showed a double feature corresponding to the melting and subsequent decomposition of remaining NaBH_4 for the samples in the first group. These were both hydrogen release events, with less gas being released during melting in the case of MnF_3 . This was also corroborated by TPD. For ScF_3 and CeF_3 , the melting regions were made of more than one feature in the DSC-Netzsch data. The extra features were not seen by TPD and therefore corresponded to phase transformations without gas release.



(a) Group 1



(b) Group 2



(c) Group 3

Figure 4. Cont.

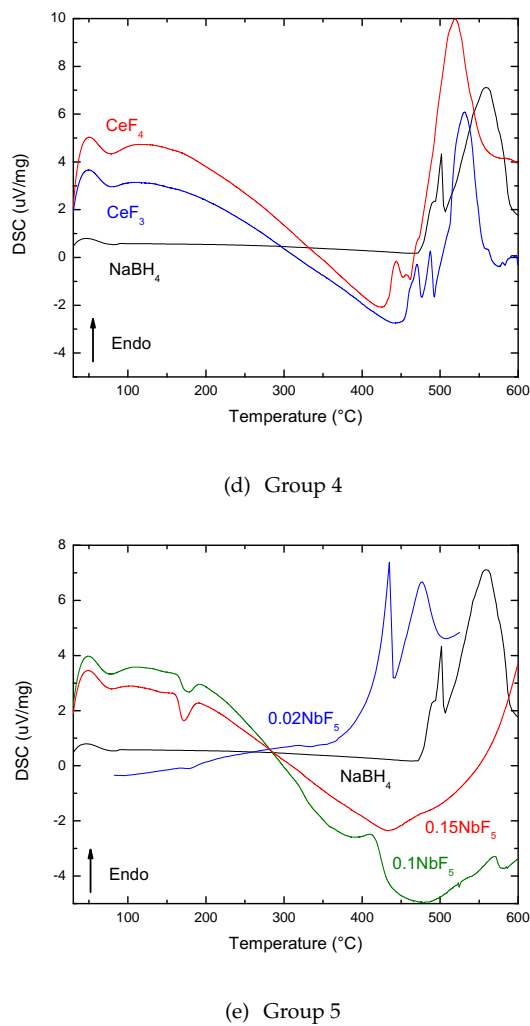


Figure 4. DSC-Netzsch corresponding to the samples distributed in the same different groups as in Figure 3. The numbers on the right-hand side indicate the shift applied to the data for plotting.

From this group of samples, NbF_5 was the one with the lowest melting point and the lowest decomposition temperature for the remaining NaBH_4 , in agreement with both TPD and DSC-Setaram results.

The second group of samples showed a heterogeneous behavior in DSC-Nezsch (Group 2 in Figure 4). This was consistent with the results by TPD and DSC-Setaram showing the variety of interactions between the different TM fluorides and NaBH_4 . Like in the previous group, the presence of extra features in the melting area mostly indicated phase transformations without gas release, except for ZnF_2 and NiF_2 , which showed a TPD shoulder at lower temperatures than the melting of the NaBH_4 feature. These features corresponded to the growing shoulder observed by DSC-Setaram in Figure 3.

The group made of CrF_3 and AgF showed the presence of extra DSC features below the melting temperature of NaBH_4 in both Setaram and Netzschi data. In the case of CrF_3 , the lowest temperature feature corresponded with a gas release shoulder in TPD, while the event in AgF was a phase transformation without gas release. An extra feature at 580 °C for CrF_3 was only seen by DSC-Netzschi. This also corresponded to a phase transformation without gas release.

The comparison between CeF_3 and CeF_4 confirmed the results by DSC-Setaram about the lower oxidation state being less efficient to decrease the melting and decomposition temperatures of NaBH_4 (Group 4 in Figure 4). Higher oxidation state systems such as CeF_4 packed more F^- ions around the Ce^+ compared to CeF_3 . This caused a decrease of the melting point from 817 to 650 °C that made the TMF more susceptible to reactions with NaBH_4 during milling. This coincided with the fact that the additive with the highest oxidation state, NbF_5 , resulted in some of the lowest hydrogen melting and desorption temperatures observed. On the other hand, the increase of NbF_5 content in the mixture led to the decrease of the intensity of the melting and decomposition features. For 15 mol% of NbF_5 , the DSC features were lost (Group 5 in Figure 4).

2.3. Thermogravimetric Analysis

The TGA data showed that for most of the samples, significant mass losses did not start until about 470 °C (see Figure A2 in Appendix A). The most notable exceptions were the NbF_5 and NiF_2 samples starting at about 400 °C. Below this temperature, the largest mass loss was seen for NbF_5 , 10 and 15 mol%, with 3.5 and 3.6 wt%, respectively, and for CeF_4 , with 1.4 wt%. All other samples showed mass losses below 1 wt% for the same temperature range. Based on the TPD and DSC results, the mass loss observed below the melting of NaBH_4 was related to intermediate phases formed during the heating process involving NaBH_4 .

For the samples containing 2 mol% of TM fluoride, the largest mass evolution between 300 and 600 °C was seen for the YF_3 case (31.3 wt%), while the smallest mass loss was seen for the CoF_3 sample (16.4 wt%) (Figure 5). These mass losses were larger than the gravimetric capacity of NaBH_4 (10.6 wt%).

Thus, the mass loss in this temperature range included gas released during melting and decomposition of NaBH_4 , as well as gas release events related to other phases formed by the reaction of the fluoride and the borohydride. This might include a substantial evaporation of Na [43].

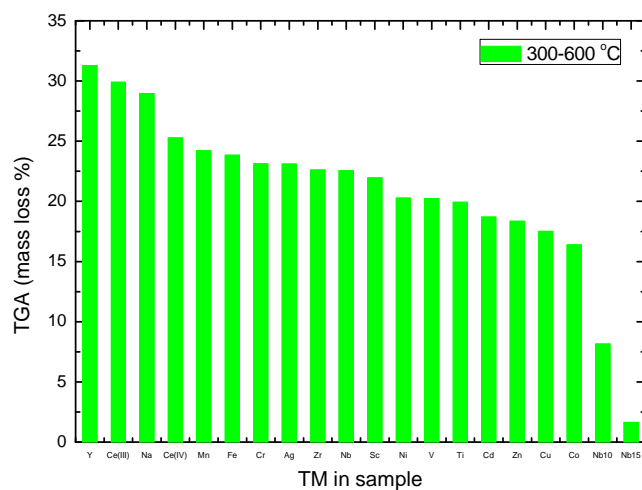


Figure 5. TGA data showing the mass loss between 300 and 600 °C for the samples with additive.

The difference between CeF_3 and CeF_4 was a decrease of the mass loss for the higher oxidation state: 30 to 25.3 wt% between 300 and 600 °C. When increasing the amount of NbF_5 from 2 to 15 mol%, the mass loss went from 22.5 to 1.6 wt% in the same temperature range. This indicated that for the higher content of NbF_5 , a larger portion of the hydrogen contained in the mixture with NaBH_4 was released during the ball milling process due to the low melting point of the fluoride. In order to increase the hydrogen yield, the amount of NbF_5 had to be lower than 2 mol%, which would also affect the melting and decomposition temperatures.

The TGA data showed that even if NbF_5 was one of the most efficient additives to decrease the melting and decomposition temperatures of NaBH_4 , as seen by TPD and DSC, its usefulness for hydrogen storage was hindered by its reactive behavior and the small yield of hydrogen obtained from the milled mixture. The results also showed that a TM fluoride such as MnF_3 produced a desirable destabilization of NaBH_4 , while still giving high hydrogen yields of 24.2 wt% between 300 and 600 °C (Table 3).

Table 3. Mass loss measured by TG in the 100–300 °C and 300–600 °C temperature ranges. The tabulated values correspond to the minima of the measured data in every region. Samples are ordered from larger to smaller losses following Figure 5.

Sample	TG Mass Loss % 100–300 °C	TG Mass Loss % 300–600 °C
NaBH_4		14.0
YF_3	0.7	31.3
CeF_3	0.3	29.9
CeF_4	1.4	25.3
MnF_3	0.2	24.2
FeF_3	0.4	24.0
CrF_3	0.1	23.1
AgF	0.3	23.1
ZrF_4	0.4	22.6
NbF_5 (2 mol%)	0.3	22.5
ScF_3	0.3	22.0
NiF_2	0.6	20.3
VF_4	0.1	20.2
TiF_4	0.3	20.0
CdF_2	0.9	19.0
ZnF_2	0.2	18.3
CuF_2	0.5	17.5
CoF_3	0.4	16.4
NbF_5 (10 mol%)	3.5	8.2
NbF_5 (15 mol%)	3.6	1.6

3. Materials and Methods

Mixtures containing pure NaBH_4 (Sigma Aldrich, 99%) and a commercially available anhydrous transition metal fluoride (TMF, Sigma Aldrich: in 1:0.02 molar ratios (2 mol%)) were ball milled in Ar atmosphere using a Fritzch Pulverisette 7 Planetary Mill (300 rpm) and hardened stainless steel vials and balls (Table 4). The samples included the complete first period TM and the available YF_3 , ZrF_4 , NbF_5 , AgF , and CdF_2 from the second period, as well as CeF_3 and CeF_4 . The lanthanide metal Ce was chosen due to its light weight. In the NbF_5 case, additional molar ratios of 1:0.10 and 1:0.15 (10 and 15 mol%) were also prepared to study the destabilization effect of increasing the amount of additive. The fluoride name was used throughout the text to identify the $\text{NaBH}_4 + \text{TMF}$ mixture.

All the samples were treated equally and were milled for 1 h with a ball-to-powder ratio of 40:1. Both hardened stainless steel vials and balls (10 mm ϕ) were used for the milling. Sample handling was carried out in MBraun Unilab glove boxes filled with purified argon (<1 ppm O_2 , H_2O) to avoid contamination.

Powder X-ray diffraction (PXD) patterns were collected in transmission mode using CuK α radiation ($\lambda = 1.5418 \text{ \AA}$) in a Bruker AXS D8 Advance Diffractometer equipped with a Göbel mirror and a LynxEyeTM 1D strip detector. The samples were packed in sealed boron glass capillaries (0.5 and 0.8 mm ϕ) in Ar atmosphere. These were kept rotating during measurements to decrease preferred directionality effects. Small amounts of pure Si were added to some samples as internal standard (ABCR, APS 1-5 micron, 99.999%) to determine the instrumental off-set. Acquisition of data were restricted to the $2\theta = 5\text{--}80^\circ$ range, with $\Delta 2\theta = 0.02^\circ$ and 2 s/step scanning rates.

Differential scanning calorimetry (DSC) measurements were performed both in a Setaram Sensys DSC and a Netzsch STA 449 F3 Jupiter instrument that also performed simultaneous Thermogravimetric Analysis (TGA). In the Setaram case, 50 mg of sample were put into high pressure stainless steel crucibles that were heated up to 600 °C with an Ar flow of 15 ml/min and a heating rate of 2 °C/min. For the simultaneous TGA and DSC experiments performed in the Netzsch instrument, 3 to 5 mg samples were placed in Al crucibles with pierced lids and heated between 30 and 600 °C, with a heating rate of 2 °C/min under argon gas flow (100 mL/min).

The different experimental conditions of the DSC experiments were chosen to provide as much complementary information as possible on the effects induced by the TM fluorides on the NaBH₄.

Additional temperature-programmed desorption (TPD) with residual gas analysis (RGA) data were collected from approximately 25 mg of sample with an in-house built setup under vacuum conditions (10^{-5} mbar). Heating ramps between RT and 600 °C at a constant heating rate of 2 °C/min were used. RGA data were obtained with a MULTIVISON IP detector system coupled to a PROCESS Eye analysis package from MKS Instruments.

Table 4. Relevant transition metal fluorides data. Enthalpy values (for the solid phase) from the Peep Database [44].

4. Conclusions

Transition metal fluorides from the first and second periods of the periodic table milled with NaBH₄ in a 0.02:1 molar ratio exhibited a destabilizing effect that led to the decrease of the melting and the decomposition temperatures of the borohydride below 505 °C and 535 °C, respectively.

- In particular, NbF₅ and MnF₃ were very good destabilizers of NaBH₄, with a 30 °C decrease of its melting temperature and a 50 to 57 °C decrease of its decomposition temperature, while still giving high decomposition gas yields in the 300 and 600 °C region of 24.2 and 22.5 wt%, for 2 mol% of MnF₃ and NbF₅, respectively, that might include evaporation of Na.
- In addition, the strong reactivity of NbF₅ meant that the yield of hydrogen from a mixture with NaBH₄ decreased strongly with increasing fluoride amount (1.6 wt%, for 15 mol% of NbF₅), since most of the hydrogen was lost during the ball milling process.
- Increasing the additive amount from 2 to 10 and 15 mol% led to the loss of the NaBH₄ and therefore the loss of hydrogen yield during thermal decomposition.
- Higher oxidation states of the metal in the fluoride were more efficient in reducing the melting and decomposition temperatures of NaBH₄. This was confirmed by the comparison between CeF₃ and CeF₄ (506 and 502 °C, respectively), but also by the results showing NbF₅, the TM fluoride with highest oxidation state, being one of the most efficient destabilizers.
- An increase of the oxidation state also seemed to lead to a decrease of the gas yield in the 300 and 600 °C region, with 29.9 and 25.3 wt%, for CeF₃ and CeF₄, respectively).

It was found that the destabilizing performance of the studied fluorides depended on a combination of their properties rather than on a single parameter. Higher fluoride melting points required higher energy ball milling conditions than lower melting points to achieve similar chemical interactions with NaBH₄ during ball milling, while smaller enthalpies of formation and higher metal oxidation values enhanced the chemical interaction further during and after the ball milling process.

Future studies are envisioned to understand how the different properties act on the most successful fluorides found in this work.

Author Contributions: The conceptualization and methodology for this article were carried out by I.L.J. and G.N.K. Experimental investigation and part of the formal analysis were carried out by K.N. and G.N.K. Validation, formal analysis, data curation, project administration, provision of materials, supervision, visualization, and writing of the original draft were carried out by I.L.J. The review of the manuscript was by G.N.K. and B.C.H. Overall resources and funding acquisition were by B.C.H. All authors have read and agreed to the published version of the manuscript.

Funding: Financial support from the Research Council of Norway and the FLYHY project (Contract No. 226943), under the FP7 Program in the European Commission, is gratefully acknowledged.

Conflicts of Interest: The authors declare no conflict of interest. The funders had no role in the design of the study; in the collection, analyses, or interpretation of data; in the writing of the manuscript; nor in the decision to publish the results.

Abbreviations

The following abbreviations are used in this manuscript:

MDPI	Multidisciplinary Digital Publishing Institute
DOAJ	Directory of open access journals
PEMFCs	proton exchange membrane fuel cells
DBFCs	direct boron hydride fuel cells
TM	transition metals
PXD	powder X-ray diffraction
DSC	differential scanning calorimetry
TPD	temperature-programmed desorption
TMF	transition metal fluorides
TGA	thermogravimetric analysis

RT room temperature
RGA residual gas analyzer

Appendix A

Appendix A.1. PXD Data in Plots, Separated into Groups

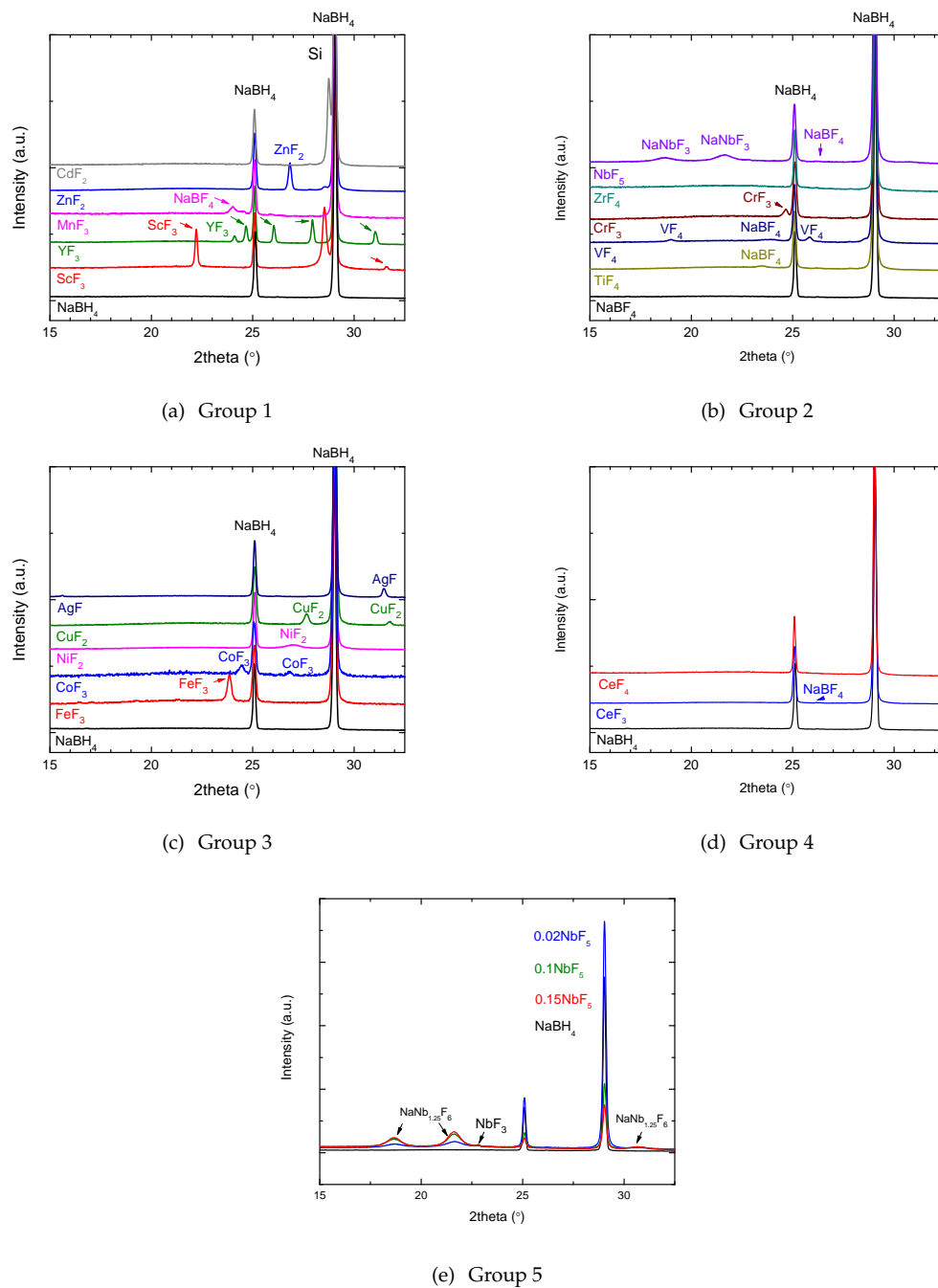
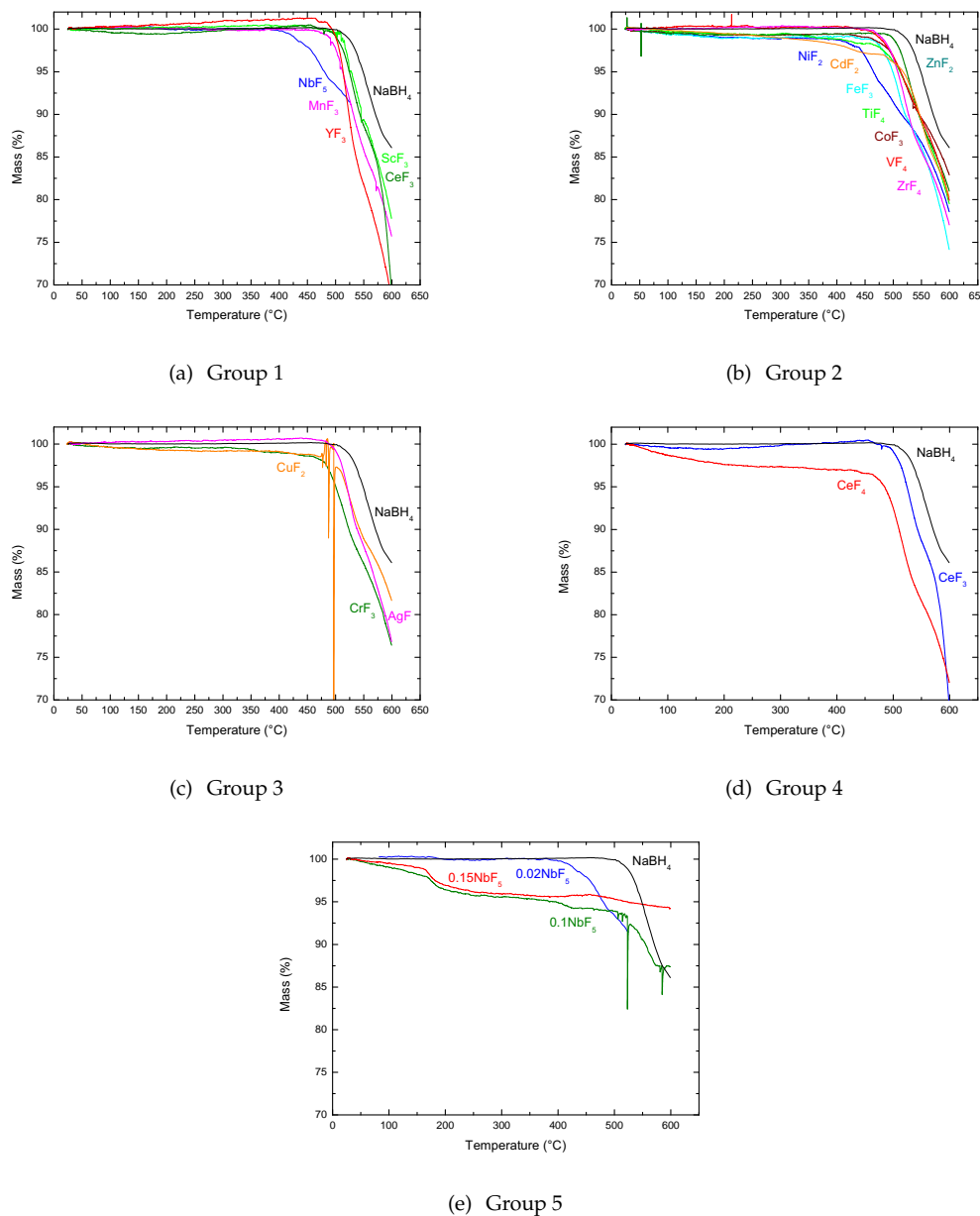


Figure A1. PXD data corresponding to the samples distributed in the different groups discussed in the text.

Appendix A.2. TGA Data in Plots, Separated into Groups

**Figure A2.** TGA corresponding to the samples distributed in the different groups discussed in the text.

References

- Varin, R.A.; Bidabadi, A.S. Nanostructured, complex hydride systems for hydrogen generation. *AIMS Energy* **2015**, *3*, 121–143. [[CrossRef](#)]
- Xin, L.; Chuan, W.; Feng, W. Light metal complex hydride hydrogen storage systems. *Prog. Chem.* **2015**, *27*, 1167–1181.
- Callini, E.; Atakli, Z.Ö.K.; Hauback, B.C.; Orimo, S.I.; Jensen, C.; Dornheim, M.; Grant, D.; Cho, Y.W.; Chen, P.; Hjörvarsson, B.; et al. Complex and liquid hydrides for energy storage. *Appl. Phys. A* **2016**, *122*, 353. [[CrossRef](#)]
- Orimo, S.I.; Nakamori, Y.; Eliseo, J.R.; Züttel, A.; Jensen, C.M. Complex hydrides for hydrogen storage. *Chem. Rev.* **2007**, *107*, 4111–4132. [[CrossRef](#)] [[PubMed](#)]
- Mohtadi, R.; Orimo, S.I. The renaissance of hydrides as energy materials. *Nat. Rev. Mater.* **2017**, *2*, 16091. [[CrossRef](#)]

6. Frommen, C.; Sørby, M.H.; Heere, M.; Humphries, T.; Oslen, J.E.; Hauback, B.C. Rare earth borohydrides-crystal structures and thermal properties. *Energies* **2017**, *10*, 2115. [[CrossRef](#)]
7. Milanese, C.; Jensen, T.R.; Hauback, B.C.; Pistidda, C.; Dornheim, M.; Yang, H.; Lombardo, L.; Zuetel, A.; Filinchuk, Y.; Ngene, P.; et al. Complex hydrides for energy storage. *Int. J. Hydrogen Energy* **2019**, *44*, 7860–7874. [[CrossRef](#)]
8. Humphries, T.D.; Kalantzopoulos, G.N.; Llamas-Jansa, I.; Olsen, J.E.; Hauback, B.C. Reversible Hydrogenation Studies of NaBH₄ Milled with Ni-Containing Additives. *J. Phys. Chem. C* **2013**, *117*, 6060–6065. [[CrossRef](#)]
9. Llamas-Jansa, I.; Friedrichs, O.; Fichtner, M.; Bardaji, E.G.; Züttel, A.; Hauback, B.C. The Role of Ca(BH₄)₂ Polymorphs. *J. Phys. Chem. C* **2012**, *116*, 13472–13479. [[CrossRef](#)]
10. Albanese, E.; Kalantzopoulos, G.N.; Vitillo, J.G.; Pinatet, E.; Civalleri, B.; Deledda, S.; Bordiga, S.; Hauback, B.C.; Baricco, M. Theoretical and experimental study on Mg(BH₄)₂-Zn(BH₄)₂ mixed borohydrides. *J. Alloy. Compd.* **2013**, *580*, MH2012. [[CrossRef](#)]
11. Kalantzopoulos, G.; Vitillo, J.; Albanese, E.; Pinatet, E.R.; Civalleri, B.; Deledda, S.; Bordiga, S.; Baricco, M.; Hauback, B.H. Hydrogen storage of Mg-Zn mixed metal borohydrides. *J. Alloys Compd.* **2014**, *615* (Suppl. 1), S702–S705. [[CrossRef](#)]
12. Paskevicius, M.; Jepsen, L.H.; Schouwink, P.; Černý, R.; Ravnsbæk, D.B.; Filinchuk, Y.; Dornheim, M.; Besenbacher, F.; Jensen, T.R. Metal borohydrides and derivatives – synthesis, structure and properties. *Chem. Soc. Rev.* **2017**, *46*, 1565–1634. [[CrossRef](#)]
13. Züttel, A.; Wenger, P.; Rentsch, S.; Sudan, P.; Mauron, P.; Emmenegger, C. LiBH₄ a new hydrogen storage material. *J. Power Sources* **2003**, *118*, 1–7. [[CrossRef](#)]
14. Zavorotynska, O.; El-Kharbachi, A.; Deledda, S.; Hauback, B.C. Recent progress in magnesium borohydride Mg(BH₄)₂: Fundamentals and applications for energy storage. *Int. J. Hydrogen Energy* **2016**, *41*, 14387–14403. [[CrossRef](#)]
15. Pottmaier, D.; Baricco, M. Materials for hydrogen storage and the Na-Mg-B-H system. *AIMS Energy* **2015**, *3*, 75–100. [[CrossRef](#)]
16. Urgnani, J.; Torres, F.J.; Palumbo, M.; Baricco, M. Hydrogen release from solid state NaBH₄. *Int. J. Hydrogen Energy* **2008**, *33*, 3111–3115. [[CrossRef](#)]
17. National Renewable Energy Laboratory. *Go/No-Go Recommendation for Sodium Borohydride for on-Board Vehicular Hydrogen Storage*; Technical Report; Review Panel Recommendation Report; U.S. Department of Energy (DoE): Washington, DC, USA, 2007.
18. Santos, D.; Sequeira, C. Sodium borohydride as a fuel for the future. *Renew. Sustain. Energy Rev.* **2011**, *15*, 3980–4001. [[CrossRef](#)]
19. Kim, T.; Kwon, S. Design and development of a fuel cell-powered small unmanned aircraft. *Int. J. Hydrogen Energy* **2012**, *37*, 615–622. [[CrossRef](#)]
20. Mao, J.; Gregory, D.H. Recent Advances in the Use of Sodium Borohydride as a Solid State Hydrogen Store. *Energies* **2015**, *8*, 430–453. [[CrossRef](#)]
21. Kwon, S.; Kim, M.J.; Kang, S.; Kim, T. Development of a high-storage-density hydrogen generator using solid-state NaBH₄ as a hydrogen source for unmanned aerial vehicles. *Appl. Energy* **2019**, *251*, 113331. [[CrossRef](#)]
22. Llamas-Jansa, I.; Aliouane, N.; Deledda, S.; Fonneløp, J.E.; Frommen, C.; Humphries, T.; Lieutenant, K.; Sartori, S.; Sørby, M.H.; Hauback, B.C. Chloride substitution induced by mechano-chemical reactions between NaBH₄ and transition metal chlorides. *J. Alloys Compd.* **2012**, *530*, 186–192. [[CrossRef](#)]
23. Kalantzopoulos, G.N.; Guzik, M.N.; Deledda, S.; Heyn, R.H.; Muller, J.; Hauback, B.C. Destabilization effect of transition metal fluorides on sodium borohydride. *Phys. Chem. Chem. Phys.* **2014**, *16*, 20483–20491. [[CrossRef](#)] [[PubMed](#)]
24. Zhang, B.J.; Liu, B.H.; Li, Z.P. Destabilization of LiBH₄ by (Ce, La)(Cl, F)3 for hydrogen storage. *J. Alloys Compd.* **2011**, *509*, 751–757. [[CrossRef](#)]
25. Al-Kukhun, A.; Hwang, H.T.; Varma, A. NbF₅ additive improves hydrogen release from magnesium borohydride. *Int. J. Hydrogen Energy* **2012**, *37*, 17671–17677. [[CrossRef](#)]
26. Zhang, Z.G.; Wang, H.; Liu, J.W.; Zhu, M. Thermal decomposition behaviors of magnesium borohydride doped with metal fluoride additives. *Thermochim. Acta* **2013**, *560*, 82–88. [[CrossRef](#)]

27. Minella, C.B.; Garroni, S.; Pistidda, C.; Baro, M.D.; Gutfleisch, O.; Klassen, T.; Dornheim, M. Sorption properties and reversibility of Ti(IV) and Nb(V)-fluoride doped-Ca(BH₄)₂-MgH₂ system. *J. Alloys Compd.* **2015**, *622*, 989–994. [CrossRef]
28. Zhou, H.; Zhang, L.; Gao, S.; Liu, H.; Xu, L.; Wang, X.; Yan, M. Hydrogen storage properties of activated carbon confined LiBH₄ doped with CeF₃ as catalyst. *Int. J. Hydrogen Energy* **2017**, *42*, 23010–23017. [CrossRef]
29. Richter, B.; Ravnsbaek, D.B.; Sharma, M.; Spyratou, A.; Hagemann, H.; Jensen, T.R. Fluoride substitution in LiBH₄: destabilization and decomposition. *Phys. Chem. Chem. Phys.* **2017**, *19*, 30157–30165. [CrossRef]
30. Rude, L.H.; Filsø, U.; D’Anna, V.; Spyratou, A.; Richter, B.; Hino, S.; Zavorotynska, O.; Baricco, M.; Sørby, M.H.; Hauback, B.C.; et al. Hydrogen–fluorine exchange in NaBH₄–NaBF₄. *Phys. Chem. Chem. Phys.* **2013**, *15*, 18185–18194. [CrossRef]
31. Chong, L.; Zou, J.; Zeng, X.; Ding, W. Effects of La fluoride and La hydride on the reversible hydrogen sorption behaviors of NaBH₄: A comparative study. *J. Mater. Chem. A* **2014**, *2*, 8557–8570. [CrossRef]
32. Huang, T.; Zou, J.; Zhao, N.; Zeng, X.; Ding, W. Reversible hydrogen storage system of 3NaBH₄–0.5ScF₃–0.5YF₃: The synergistic effect of ScF₃ and YF₃. *J. Alloys Compd.* **2019**, *791*, 1270–1276. [CrossRef]
33. Zhao, N.; Zou, J.; Zeng, X.; Ding, W. Mechanisms of partial hydrogen sorption reversibility in a 3NaBH₄/ScF₃ composite. *RSC Adv.* **2018**, *8*, 9211–9217. [CrossRef]
34. Huang, T.; Zou, J.; Meng, F.; Wang, J.; Liu, H.; Ding, W. Reversible hydrogen sorption behaviors of the 3NaBH₄–(x)YF₃–(1 – x)GdF₃ system: The effect of double rare earth metal cations. *Int. J. Hydrogen Energy* **2019**. [CrossRef]
35. Jain, A.; Agarwal, S.; Ichikawa, T. Catalytic Tuning of Sorption Kinetics of Lightweight Hydrides: A Review of the Materials and Mechanism. *Catalysts* **2018**, *8*, 651. [CrossRef]
36. Mao, J.; Guo, Z.; Nevirkovets, I.; Liu, H.; Dou, S. Hydrogen De-/Absorption Improvement of NaBH₄ Catalyzed by Titanium-Based Additives. *J. Phys. Chem. C* **2011**, *116*, 1596–1604. [CrossRef]
37. Nakagawa, Y.; Lee, C.H.; Matsui, K.; Kousaka, K.; Isobe, S.; Hashimoto, N.; Yamaguchi, S.; Miyaoka, H.; Ichikawa, T.; Kojima, Y. Doping effect of Nb species on hydrogen desorption properties of AlH₃. *J. Alloys Compd.* **2018**, *734*, 55–59. [CrossRef]
38. Malka, I.E.; Bystrzycki, J. The effect of storage time on the thermal behavior of nanocrystalline magnesium hydride with metal halide additives. *Int. J. Hydrogen Energy* **2014**, *39*, 3352–3359. [CrossRef]
39. Malka, I.; Czujko, T.; Bystrzycki, J. Catalytic effect of halide additives ball-milled with magnesium hydride. *Int. J. Hydrogen Energy* **2010**, *35*, 1706–1712. [CrossRef]
40. Jin, S.A.; Shim, J.H.; Cho, Y.W.; Yi, K.W. Dehydrogenation and hydrogenation characteristics of MgH₂ with transition metal fluorides. *J. Power Sources* **2007**, *172*, 859–862. [CrossRef]
41. Luo, Y.; Wang, P.; Ma, L.P.; Cheng, H.M. Hydrogen sorption kinetics of MgH₂ catalyzed with NbF₅. *J. Alloys Compd.* **2008**, *453*, 138–142. [CrossRef]
42. Nakagawa, Y.; Zhang, T.; Kitamura, M.; Isobe, S.; Hino, S.; Hashimoto, N.; Ohnuki, S. A Systematic Study of the Effects of Metal Chloride Additives on H₂ Desorption Properties of Ammonia Borane. *J. Chem. Eng. Data* **2016**, *61*, 1924–1929. [CrossRef]
43. Kumar, S.; Jain, A.; Miyaoka, H.; Ichikawa, T.; Kojima, Y. Study on the thermal decomposition of NaBH₄ catalyzed by ZrC₁₄. *Int. J. Hydrogen Energy* **2017**, *42*, 22432–22437. [CrossRef]
44. Roine, A. *Peep Database, HSC Outkumpu Chemistry for Windows*; Vs. 5.1; 02103-ORC-T; Schlumberger Limited: Honston, TX, USA, 2002; ISBN 952-9507-08-9.

Sample Availability: Samples of the compounds are not available from the authors. They were destroyed due to age.



© 2020 by the authors. Licensee MDPI, Basel, Switzerland. This article is an open access article distributed under the terms and conditions of the Creative Commons Attribution (CC BY) license (<http://creativecommons.org/licenses/by/4.0/>).